ンパク質に特異的な抗体を用いたアフィニティークロマトグラフィーカラムなどが開発されている。２２のタンパク質が何れも５０KDa 以上の蛋白であることから、我々は東レ株式会社が開発中の中空繊維（ホロファイバー）を用いた低分子分画装置を利用して、低分子量領域に絞って、微量成分の分画を試みている（図４）。硝子体プロテオームは血漿プロテオームで蓄積されたノウハウを応用して微量タンパク質の同定が今後盛んに行われると予想される。

　　　日本は硝子体プロテオームでこれまで世界をリードしており、これまでに報告された４つのパイオニア的な硝子体プロテオーム研究をご紹介したい。２００２年、中西等は糖尿病網膜症（３検体）と黄斑円孔（２検体）の患者の硝子体それぞれ２次元電気泳動で分画し、質量分析計（MALDI-TOF-MS、ESI-MS/MS）で分析した結果、５０種類の蛋白を同定し、この内の３０は血漿には含まれていないことを明らかにした。IgG、α-antitrypsin、 α-2-HS glycoprotein、complement C4 断片が糖尿病の硝子体で増加していることを報告している（文献１）。２００３年小山等は糖尿病網膜症患者の硝子体を１次元電気泳動で分画し、質量分析計（ESI-IT-MS/MS）で分析した結果、８４種類の蛋白の同定に成功し、前年に行った２次元電気泳動と合わせて１２１種類のタンパク質の同定に成功している。４種類の血管促進因子と３種類の抑制因子、PEDF、endostatin、thrombospondin が検出されている（文献２）。また同年、山根等は黄斑円孔（26 検体）の硝子体を２次元電気泳動で分画し、４００スポットを確認、７８を同定している。同定されたペプチドは１８の蛋白に由来しており、この中には PEDF、prostaglanding-D2 synthase、IRBP が含まれていた。増殖性糖尿病網膜症（３３検体）も同様に解析した結果、６００スポットを確認し、１２１を同定した結果、３８の蛋白が同定された。Enolase と Catalase が糖尿病の硝子体で顕著に増加しており、黄斑円孔の硝子体や糖尿病の血清中には検出されなかった（文献３）。2005 年には大内等によって、増殖性糖尿病初期(Pre-proliferative)で黄斑浮腫の有無（１６：４検体）の硝子体を２次元電気泳動で分画し、質量分析計（ESI-LC-MS/MS、QTOF）で分析した結果、DME のグループから１４種類の蛋白、non-DME のグループから１５種類の蛋白を同定した。特に８スポットは顕著に DME グループで増加しており、そのうちの６つのスポッは PEDF、ApoA-4、Trip-11、RPBP、VDBP と同定された（文献４）。

　　　硝子体サンプルは手術中に破棄されるものを倫理委員会の承認と文書による本人の了解を得て集められているが、検体の多くは病態末期のものが多く、これらの検体を解析しても疾患初期の硝子体内の様子を知ることができない。また、日本では正常な眼球の硝子体を集めることができないために、ベースとなるデータが不足しており、霊長類の硝子体プロテオーム解析を検討している。

３）網膜疾患の早期発見ための血漿バイオマーカーの探索

　　　近年、全ゲノム配列が解読された結果、ゲノム上には平均で１，０００塩基に１つの割合で異なる配列が存在することが明らかになった。この遺伝子多型（SNP：Single Nucleotide Polymorphism）の生理作用への影響についてはまだ明らかにされていないが、その利用方法については注目されている。ゲノム上の１つの SNP あるいは隣接する複数の SNP を組み合わせてブロックにし、これを疾患とリンクさせる試みである。同染色体に位置する

SNP の組み合わせをハプロタイプと呼ぶが、全てのハプロタイプを明らかにするために国際ハップマッププロジェクト(http://www.hapmap.org/)が進行中である。3 x 10⁹塩基から構成されるゲノム上には 1 千万個の SNP が存在すると計算されるが、これだけの SNP 数を安価に効率よく解析することは技術的に困難であった。しかし、最近、シリコンベースの DNA チップによって数十万個の SNP を同時に検出することができるようになってきた。この方法によって、すでに加齢黄斑変性の 2 つのリスク遺伝子 (CFH、Htra1)が同定されており、発症前にリスクの高い人を選別することが可能になってきた。しかし遺伝子情報からだけでは発症の時期まで予測することは困難であり、発症前の蛋白の量的・質的変化を捉えて発症を予測する方法が検討されている。発症前に健常者の硝子体を検査目的で採取することはきわめて困難であり、これを血漿や尿で代行できるか研究されている。網膜・脈絡膜から漏れた蛋白が全身への循環によって希釈されることになり、この微量な変化を検出する精度が求められる。

　　　我々は東京医科大学の西村俊秀客員教授との共同研究によって血漿蛋白の微量変化を質量分析計によって検出されるか研究している。年齢 6 5 − 8 8 歳の加齢黄斑変性患者 6 名と白内障患者 6 名の血液を採血後 3 分以内に遠心分離によって得た血漿を用いている。血漿からアルブミンと免疫グロブリンを分離して、これを 1 次元電気泳動でさらに分画しても 2 疾患の泳動パターンに差は観察されないが（図 5）、質量分析のマスクロマトグラムとマススペクトルを擬似的な 2 次表示にすると微量蛋白の変化が観察されるようになった（図 6）。我々は同様な研究を続け、発症前後の血漿サンプルによって疾患バイオマーカーの存在を検証したいと考えている。

４）質量分析計を用いたドルーゼンのプロテオーム

　　　加齢黄斑変性で観察されるドルーゼンと萎縮型や滲出型へと分岐するメカニズムは不明であるが、最近の研究によってドルーゼンの構成蛋白が明らかになり、疾患と補体との関係が注目されている。Hageman や Anderson 等は糸球体腎炎の患者で眼底所見によってドルーゼンが観察されることから、糸球体の炎症に関わる補体の活性化が網膜下でも起こっていると推測し、免疫染色法によってこれを証明している（文献 5，6，7）。さらに、Hollyfield 等もドルーゼンを抽出して、質量分析計によって蛋白組成を解析した結果、補体活性分子の存在を確認した（文献 8）。ドルーゼン内で発見された蛋白にはアミロイド β 関連分子や酸化ストレス関連分子など、補体活性化の原因になりうる蛋白が確認されている。

　　　ヒトと同様に黄斑が発達している霊長類において、1970 年代から加齢黄斑変性モデルの探索が行われてきた。独立行政法人医薬基盤研究所霊長類医科学研究センターにおいて生後 2 年でドルーゼンを発症するカニクイザルが社団法人予防衛生協会の鈴木通弘等によって発見され（文献 9）、1 頭の疾患個体から交配実験によって大家系に繁殖することに成功した（図 7）。我々は厚生労働科学研究難治性疾患克服研究事業として研究班を組織して、ヒトと同様な方法によって疾患個体のドルーゼンを抽出し、プロテオーム解析と免疫染色法によって蛋白組成を解析した。その結果、補体活性分子、抑制分子、クリスタリンなど、ヒトに類似する蛋白組成が含まれることを明らかにした。疾患サルはヒトが５０年以上かけて蓄積

するドルーゼンと同成分のドルーゼンをわずか 2 年で生成していることになる。疾患は家系内で優性遺伝することから、単一遺伝子の変異によって発症していると考えられ、この原因遺伝子の同定はドルーゼン生成のメカニズムに関わる重要な情報をもたらすと期待している。

5）黄斑のプロテオーム

　　　　霊長類と一部の鳥類などで発達している黄斑は視力を決定する重要な部位である。黄斑は錐体細胞が高密度に存在し、周辺網膜に比べて特徴ある構造をしていることから黄斑と周辺との生理的な差を分子レベルで解明するために、転写産物（RNA)の解析が行われ、黄斑特異的な遺伝子も報告されている。この研究の延長線上には黄斑の蛋白解析が考えられるが、今日まで報告されていない。その理由には 1) 一般的な実験動物であるマウスやラットには黄斑が存在しないこと、2) 黄斑部組織が微量であること、3) 新鮮な黄斑を大量に手に入れることが困難であることなどが考えられる。我々は独立行政法人医薬基盤研究所霊長類医科学研究センターにおいて研究目的に安楽死された 13−19 歳の正常なオスザル 8 頭から黄斑部と網膜周辺部を 3 mm径の円柱でくり抜き、これを 16 眼球について採取し、黄斑と周辺網膜の蛋白抽出液を準備した。これを 2 次元電気泳動によって分画し、黄斑と周辺網膜の泳動パターンから、それぞれに特異的なスポットを複数発見した（図 8）。これらのスポットをゲルからくり抜き、トリプシン処理によってペプチドに分解した後に、質量分析計（LC-MS/MS）を用いて解析した結果、これまで発見されなかった複数の蛋白が同定されてきた。黄斑疾患とこれらのタンパク質との関係については研究が続けられている。

6）網膜・硝子体プロテオーム解析の今後の課題

　　　　日進月歩の質量分析計の技術革新はこれまで不可能であった蛋白の網羅的解析を可能にし、電気泳動で分画されたスポットを容易に同定できるようになった。眼科分野でもヒトの硝子体、房水、涙液の網羅的プロテオーム解析、トランスジェニックやノックアウトマウスの眼組織のプロテオーム解析などが行われている。また、最新機器と解析ソフトを利用するとリン酸化、糖、脂質の修飾を受けた蛋白の同定や修飾されたアミノ酸の特定も可能になった。我々は黄斑に特異的な蛋白を探索する過程で、リン酸化蛋白の量的変化を観察している。蛋白修飾の生理的な意味や疾患との関係は今後明らかにされていくと期待される。このような網羅的修飾蛋白の解析はプロテオミクスによって初めて可能になった技術である。

　　　　質量分析計にも克服されなければならない弱点が存在する。その一つに質量分析計には定量性の精度が欠けることである。サンプル間に含まれる特定の蛋白について量的変化を高い精度で測定することができない。これまでは電気泳動後のバンドやスポットの濃さとして測定されたり、比較するサンプルを異なる同位体元素でそれぞれラベルして、質量分析計によってラベル化されたペプチドの検出回数として測定されたりする方法が行われてきた。同定した蛋白の定量性について今後の技術開発が望まれている。

　　　　これまで利用されてきた DNA チップを使った網羅的なトランスクリプトーム解析に加え、これにプロテオーム解析を組み合わせることによって、解析する領域を遺伝子発現から蛋白発現までに広げることが可能になった。DNA チップによって２３，０００遺伝子の変

化を観察し、同時に蛋白の有無を観察することができる。我々も同様な方法によって網膜色素上皮細胞を特異的に増殖させる因子(REF-1/TFPI-2)の作用機序を研究している（文献１０）。この研究では発現量に変化が観察された蛋白間の関係を裏付けるデータとし、遺伝子発現データから推測される遺伝子発現の連鎖反応マップを利用した。今後はここへ蛋白修飾のデータも加わり、フェノミックスの世界へ一歩一歩近づくことになると期待される。

文献

1) Nakanishi T, et al. Catalogue of soluble proteins in the human vitreous humor: comparison between diabetic retinopathy and macular hole. J Chromatogr B Analyt Technol Biomed Life Sci. 2002;776(1):89-100.

2) Koyama R, et al. Catalogue of soluble proteins in human vitreous humor by one-dimensional sodium dodecyl sulfate-polyacrylamide gel electrophoresis and electrospray ionization mass spectrometry including seven angiogenesis-regulating factors. J Chromatogr B Analyt Technol Biomed Life Sci. 2003;792(1):5-21.

3) Yamane K, et al. Proteome analysis of human vitreous proteins. Mol Cell Proteomics. 2003;2(11):1177-1187.

4) Ouchi M, et al. Proteomic analysis of vitreous from diabetic macular edema. Exp Eye Res. 2005;81(2):176-182.

5) Hageman GS, et al. Vitronectin is a constituent of ocular drusen and the vitronectin gene is expressed in human retinal pigmented epithelial cells.
FASEB J. 1999;13:477-484.

6) Mullins RF, et al. Drusen associated with aging and age-related macular degeneration contain proteins common to extracellular deposits associated with atherosclerosis, elastosis, amyloidosis, and dense deposit disease.
FASEB J. 2000;14:835-846.

7) Crabb JW, et al. Drusen proteome analysis: an approach to the etiology of age-related macular degeneration. Proc Natl Acad Sci U S A. 2002;99:14682-14687.

8) Umeda S, et al. Early-onset macular degeneration with drusen in a cynomolgus monkey (Macaca fascicularis) pedigree: exclusion of 13 candidate genes and loci. Invest Ophthalmol Vis Sci. 2005;46:683-691.

9) Umeda S, et al. Molecular composition of drusen and possible involvement of anti-retinal autoimmunity in two different forms of macular degeneration in cynomolgus monkey (Macaca fascicularis). FASEB J. 2005;19:1683-1685.

10) Shibuya M, et al. Proteomic & Transcriptomic Analyses of Retinal Pigment Epithelial Cells Exposed to REF-1/TFPI-2, a Growth Promoting Factor. Invest Ophthal Vis Sci 2007;48:516-521.
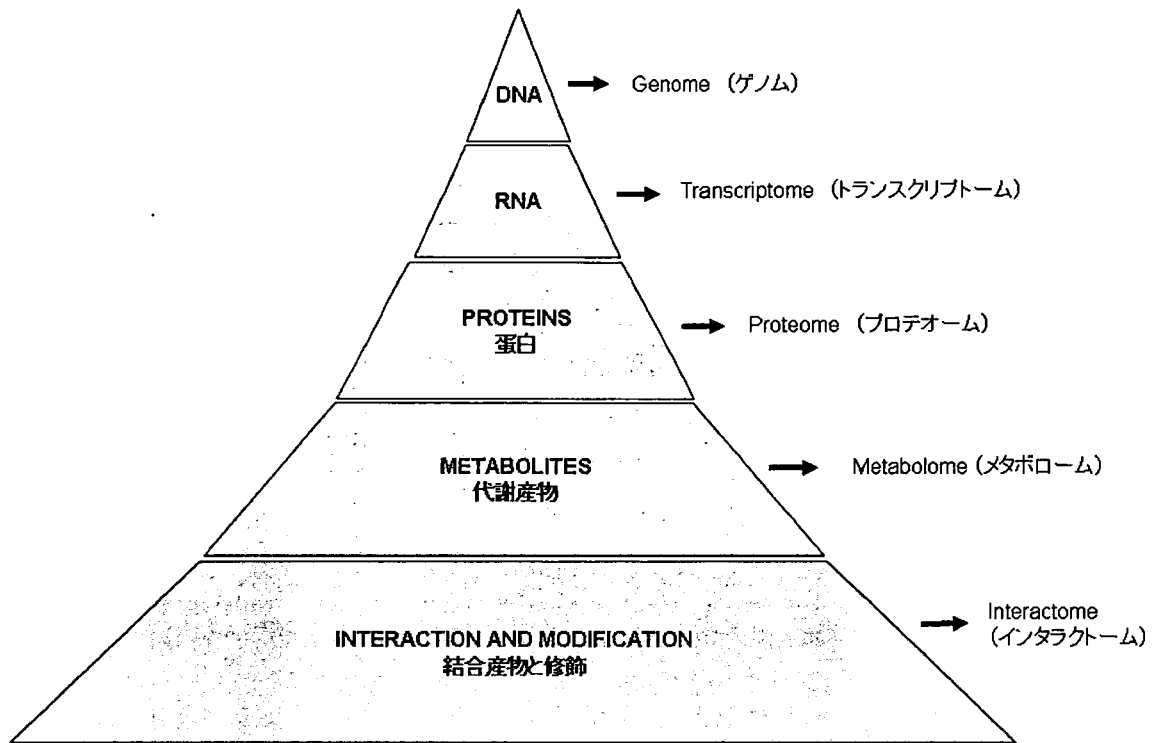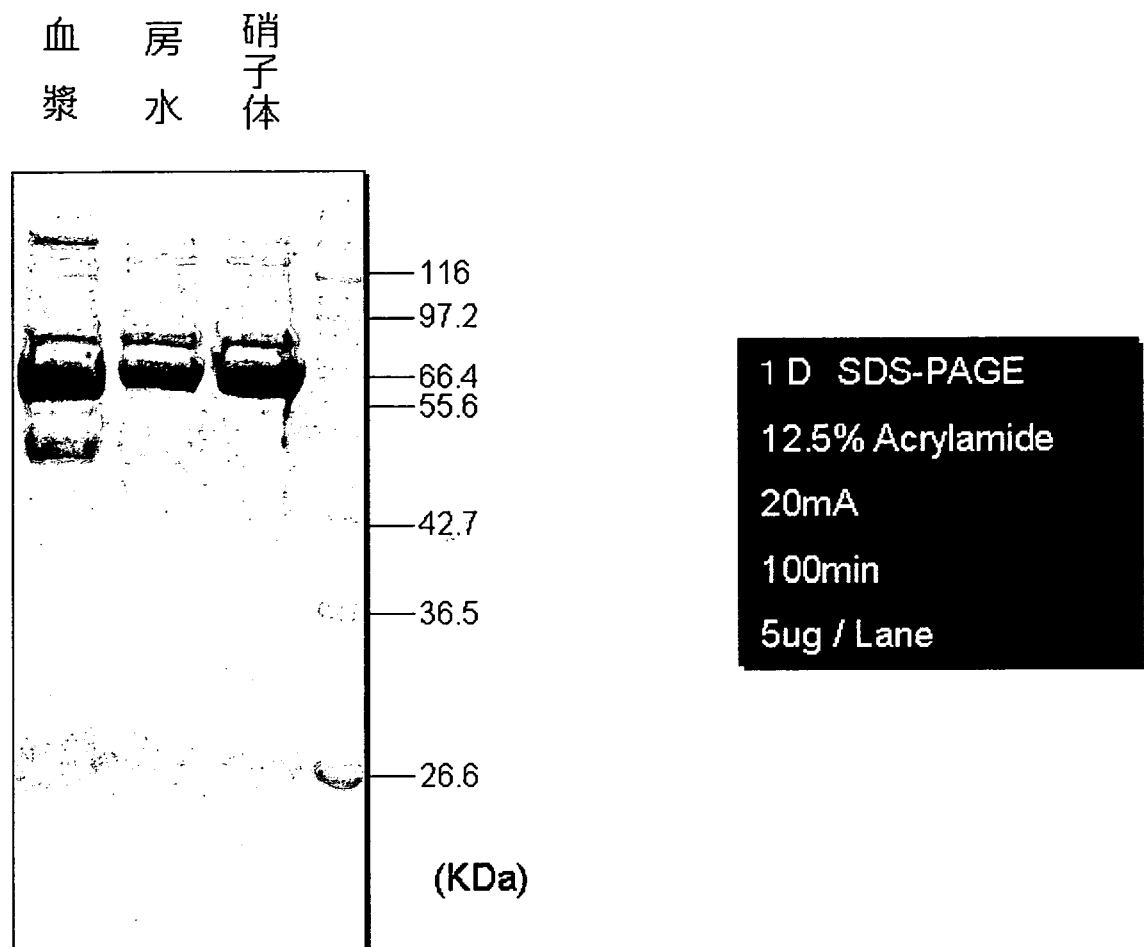
図1　生命現象の研究を総称してフェノミックスという。

血漿　房水　硝子体

	—116
	—97.2
	—66.4
	—55.6
	—42.7
	—36.5
	—26.6

(KDa)

1 D　SDS-PAGE

12.5% Acrylamide

20mA

100min

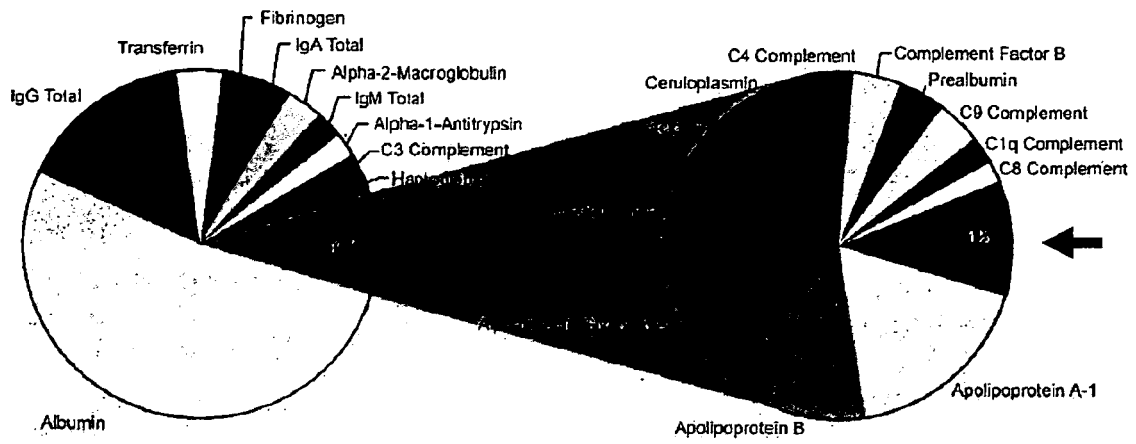5ug / Lane

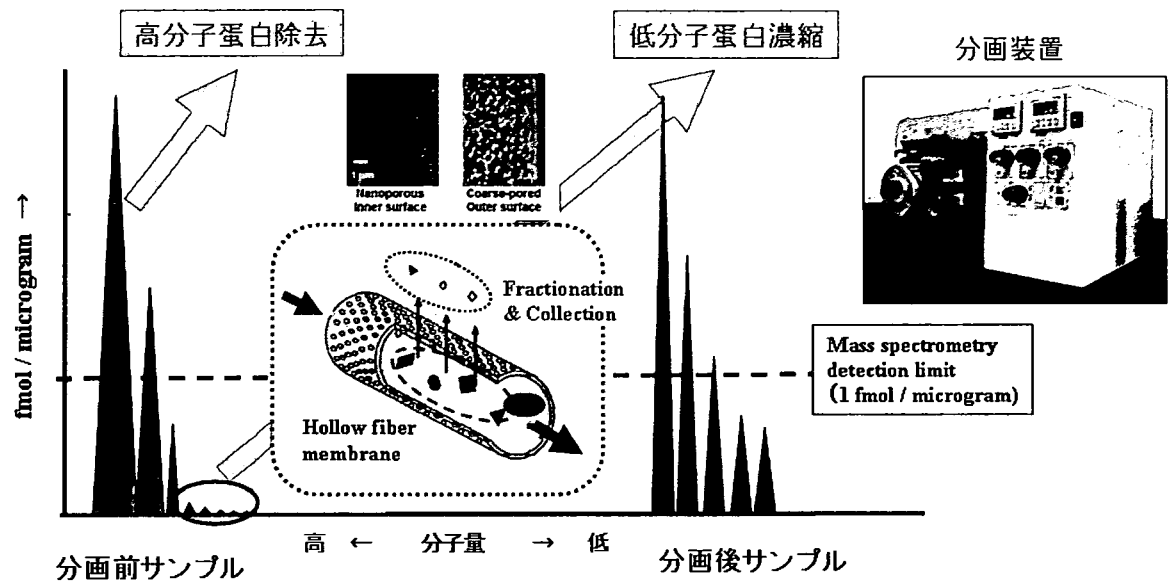図2　一次元電気泳動による血漿、房水、硝子体の分画。

図3　血漿に含まれる蛋白とその割合。２２種類のタンパク質が９９％を占める。

図4　中空紙を使った蛋白分画装置（東レ株式会社製造）による低分子量蛋白の濃縮
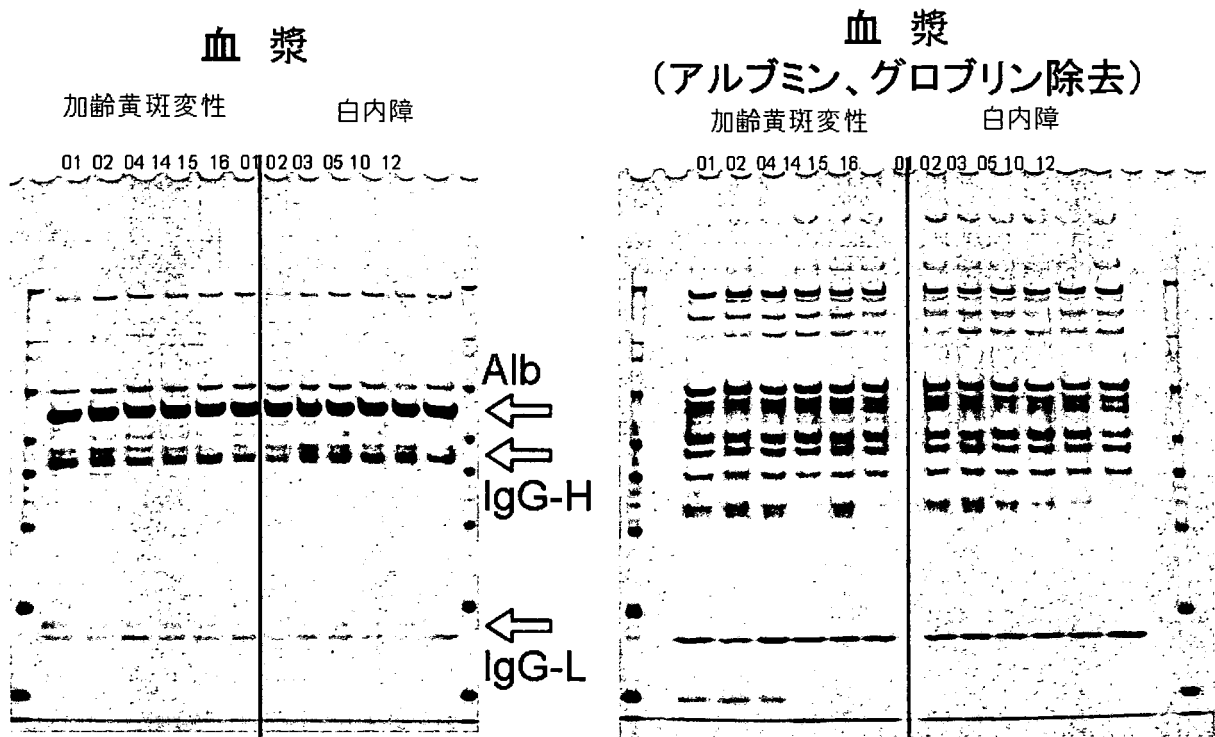
図5 血漿プロテオーム解析。加齢黄斑変性と白内障患者の血漿を一次元電気泳動によって分画した。

図6　質量分析計のマススペクトルとマスクロマトグラムによる擬似的二次元表示。蛋白量
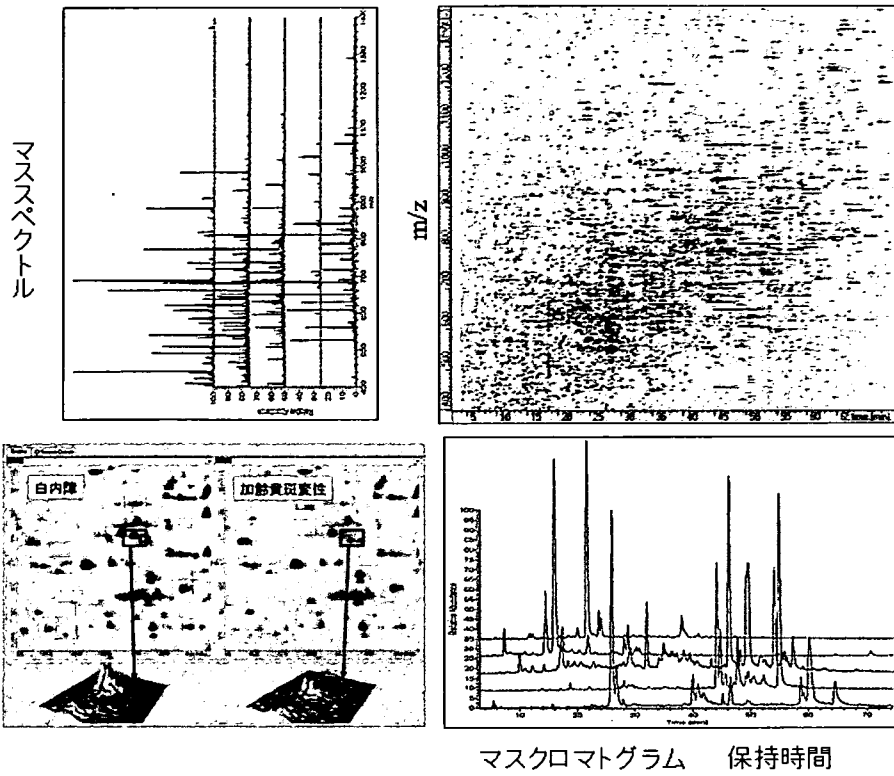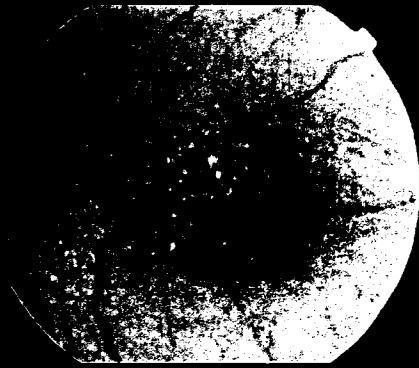はスポットの濃さとして表示される。

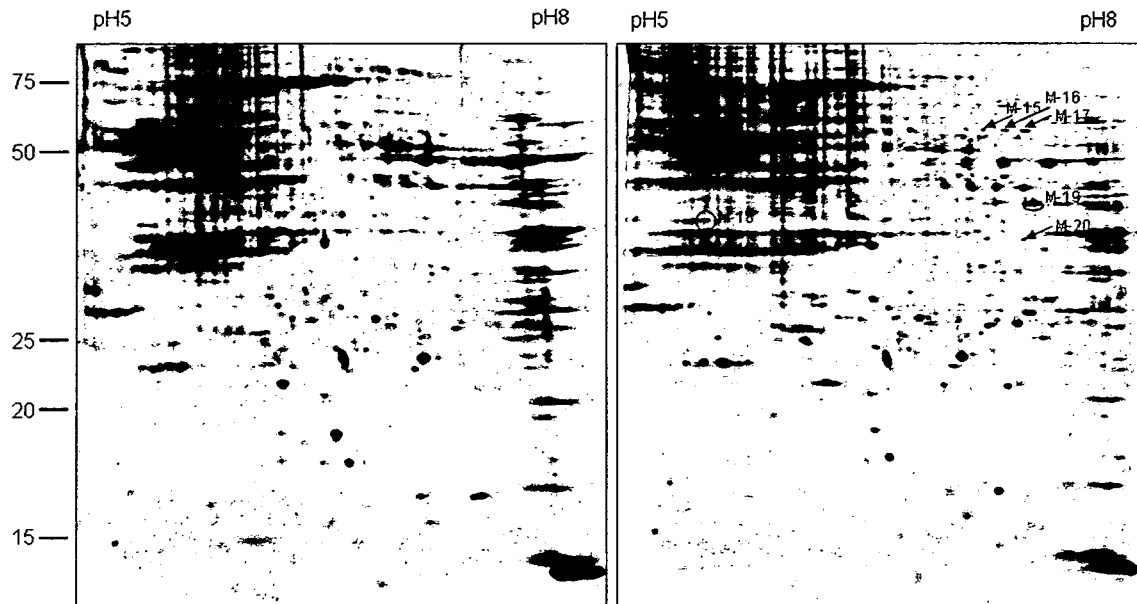図7　独立行政法人医薬基盤研究所霊長類医科学研究センターで発見された若年性黄斑変性カニクイザルの眼底写真

図8　黄斑のプロテオーム解析。網膜周辺部と黄斑の二次元電気泳動パターン。黄斑に特異的な蛋白が発見された（矢印）。

Discovery of Potential Sorbitol Dehydrogenase Inhibitors from Virtual Screening

Connie Darmanin[a], Takeshi Iwata[b], Deborah A. Carper[c] and Ossama El-Kabbani[a,*]

[a]Department of Medicinal Chemistry, Victorian College of Pharmacy, Monash University (Parkville Campus), Parkville, Victoria 3052, Australia; [b]National Institute of Sensory Organs, National Hospital Organization Tokyo Medical Center, 2-5-1 Higashigaoka, Meguro-ku, Tokyo 152-8902, Japan; [c]National Eye Institute, NIH, Bethesda MD 20892, USA

Abstract: Sorbitol dehydrogenase (SDH) is the second enzyme in the polyol pathway of glucose metabolism and is a possible target for the treatment of the complications of diabetes. In this study the molecular modelling program DOCK was used to analyse 249,071 compounds from the National Cancer Institute Database and predict those with high affinity for SDH. From a total of 21 tested the 7 compounds including flavin adenine dinucleotide disodium hydrate, (+)-Amethopterin, 3-hydroxy-2-napthoic(2-hydroxybenzylidene) hydrazide, folic acid, N-2,4-dinitrophenyl-L-cysteic acid, Vanillin azine and 1H-indole-2,3-dione,5-bromo-6-nitro-1-(2,3,4-tri-O-acetyl-α-L-arabinopyranosyl)-(9Cl), were shown to inhibit SDH and displayed IC_{50} values of 0.192 μM, 1.1 μM, 1.2 μM, 4.5 μM, 5.3 μM, 7 μM and 28 μM, respectively. These compounds may aid the design of pharmaceutical agents for the treatment of diabetes complications.

INTRODUCTION

Sorbitol dehydrogenase (SDH) is expressed in all mammalian tissues, including the brain, lens, erythrocytes and liver [1,2]. The enzyme has attracted considerable interest owing to its implication in the development of diabetic complications such as cataracts, neuropathy, retinopathy and nephropathy [3]. The structure of human SDH with and without the bound inhibitor 2-hydroxymethyl-4-(4'-N,N-dimethylaminosulfonyl-1-piperazino) pyrimidine (SDI-158) has been recently published [4]. The overall structure was found to be similar to those of rat SDH [5], NADPH-dependant whitefly ketose reductase [6], and human liver ADH [7]. The catalytic zinc atom was coordinated by His69, Cys44, Glu70 and a water molecule (tetra-coordination) in both the apo- and holoenzyme structures. In the ternary structure, penta-coordination of the zinc occurred with simultaneous interactions with the N1 nitrogen and O30 oxygen of SDI-158 and dissociation of Glu70.

Prior to the year 2000, only one known *in vivo* prototype SDH inhibitor (SDI), SDI-158, was reported in the literature. Since then the synthesis of pyridine derivatives, which had a 4'-N,N-dimethylaminosulfonyl-1-piperazino group at the 4-position and various functionalities, including hydrogen, CH₂OH, CHO, CONH₂ and CN, at the 2-position were reported [8]. The inhibitory activities of these derivatives were investigated to determine their potential as novel SDIs. The pyridine group was selected as a template because of its similarity to the pyrimidine group in SDI-158 and the various functionalities at 2-position of the pyridine ring were then used to establish structure-activity relationships. However, when tested against SDH, these compounds were

shown to be less effective inhibitors than SDI-158, hence it was concluded that the pyrimidine moiety is important for the active site interactions. New SDH inhibitors were synthesised by replacing the dimethylaminosulfonyl group in SDI-158 with a variety of heterocycles and found to inhibit SDH with the most potent IC_{50} value equal to 10 nM [9]. Based on these findings, the dimethylaminosulfonyl group was targeted and an SDI with an IC_{50} value of 4 nM that has very good drug-like properties, including a long plasma half-life, was recently reported [10].

The program DOCK (version 4.0) [11] is used to orient small molecules into potential binding sites of proteins by matching the receptor pocket to the ligand atoms or surfaces. An energy score is given based on the complementarity between the ligand and the receptor, i.e. geometry as well as overall chemical complementarity and steric fit. The docking methodology used in this study has been described in detail in the literature [12,13]. In this case, the crystal structure of the human SDH holoenzyme [4] together with the DOCK program were used to search the NCI database [14] for possible compounds that may inhibit SDH or serve as new templates for further inhibitor development.

NCI DATABASE SEARCH

The coordinates of the human SDH/NAD⁺ complex (PDB code: 1PL8) and the NCI database (249,071 compounds) were used to search for potential inhibitors or drug templates of SDH. The DOCK program [11] read 234,244 compounds, of which 230,747 compounds were docked successfully. A total number of 3,497 compounds were skipped due to the chemical and physical filters utilised by the program. This includes ignoring compounds that contain heavy atoms such as Zn, Al, Au or Ag or compounds that had too many or incorrectly assigned rotatable bonds. 15,756 compounds (6.3% of the database) were found to be chemically toxic (i.e. containing atoms such as Pt, Hg, Pu, Cr or Ir) and were also excluded from the database. Hydrogen atoms, partial

*Address correspondence to this author at the Department of Medicinal Chemistry, Victorian College of Pharmacy, Monash University (Parkville Campus), Parkville, Victoria 3052, Australia; Tel: +61 3 9903 9691; Fax: +61 3 9903 9582; E-mail: ossama.el-kabbani@vcp.monash.edu.au

charges, atomic potentials and bond orders for the complexes were assigned using the automatic procedures within the InsightII 2.1 package (Biosym Technologies Inc., San Diego, CA). Arginine, lysine, aspartate and glutamate amino acids were charged while the histidines were uncharged, with hydrogen atoms fixed at the Nε2. The Zn atom present in the active site of SDH was charged (2+). Using the program Concord the compounds were downloaded from the NCI database without altering their ionization states. Based on the SDH/SDI structure, a box was used to define the active site and included the Zn atom and Zn binding ligands. The docked compounds were restricted to the specified box. The top-ranked 3,000 compounds were checked for commercial availability using the NCI database website (www.cactus. nci.nih.gov) and only those compounds that were available were analysed thoroughly for their interactions with the active-site residues and Zn atom using the molecular modelling program InsightII (Biosym Technologies, San Diego, CA, USA). Compounds that had good interactions were then chosen for IC_{50} measurements as described below.

SDH EXPRESSION AND PURIFICATION

The coding region of human SDH (SORD) was isolated from the liver cDNA library, inserted into a prokaryotic expression vector (pET23 (+) Novagen, Madison, WI, USA) and transformed into *E. coli* BL21 (DE3) (Novagen) [15]. Briefly, SDH was purified from the supernatant by ammonium sulfate precipitation, anion exchange chromatography and affinity chromatography following established procedures [16]. The concentration, purity and enzymatic activity of SDH were examined at each step.

INHIBITORY ASSAY FOR SDH

Enzyme activity was determined using a Shimadzu UV-vis spectrophotometer (model UV160A) by following the increase in absorbance of NADH at 340 nm. SDH was tested for compound inhibition using compound stocks made up in 50% DMSO. The reaction was carried out with a 1 ml assay sample containing 42 mM glycine buffer pH 9.9, 9.9 mM D-sorbitol and 0.5 mM β-NAD^+ and different concentrations of compounds. Initially, the buffer and water were equilibrated to a constant temperature of 25° C in a hot water bath and a final concentration of DMSO in the assay not exceeding 2% was used. The reaction was commenced by addition of the substrate. One milli-unit (mU) of activity was defined as the amount of enzyme needed to oxidise 1 milli-mole of substrate per minute under initial velocity conditions at room temperature (20° C).

The DOCK program results suggested 21 compounds that may potentially inhibit SDH. These compounds were purchased and after the initial testings 7 compounds were found to be active. The active compounds included flavin adenine dinucleotide disodium hydrate, (+)-Amethopterin, 3-hydroxy-2-napthoic(2-hydroxybenzylidene) hydrazide, folic acid, N-2,4-dinitrophenyl-L-cysteic acid, Vanillin azine and 1H-indole-2,3-dione,5-bromo-6-nitro-1-(2,3,4-tri-O-acetyl-α-L-arabinopyranosyl)-(9Cl). The corresponding IC_{50} values were 0.192 μM, 1.1 M, 1.2 μM, 4.5 μM, 5.3 μM, 7 μM and 28 μM, respectively. The molecular formulae and chemical structures of the 7 active compounds are shown in Table 1.
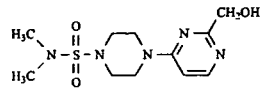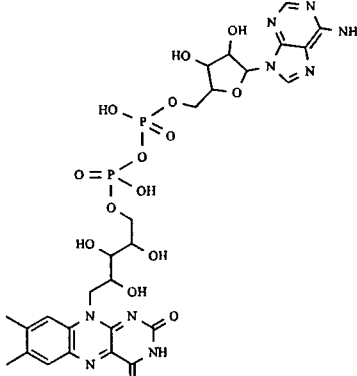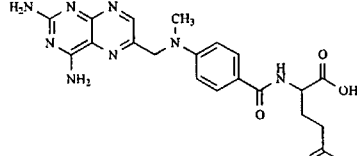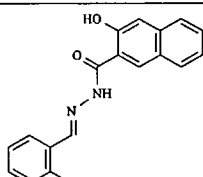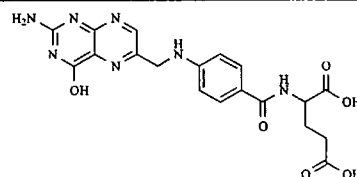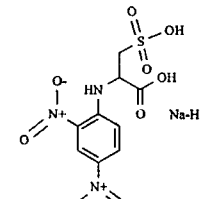
For comparison and validation of the inhibitory assay the IC_{50} value of SDI-158 was also determined and was found to be in agreement with the published value [8]. In addition, SDI-158 was docked into the active site of SDH and the resulting orientation was found to be similar to that observed in the crystal structure of the ternary complex [4]. The most potent compound, with an IC_{50} value of 0.192 μM and 5.2-fold greater potency than SDI-158, is flavin adenine dinucleotide disodium hydrate. 1H-indole-2,3-dione,5-bromo-6-nitro-1-(2,3,4-tri-O-acetyl-α-L-arabinopyranosyl)-(9Cl) was the least potent with a 28-fold less potency compared to SDI-158.

While previous studies on SDIs were focused on the design and synthesis of analogues for SDI-158 [9-12], our study revealed novel classes of potential inhibitors with *in vitro* potencies in the micro molar range. The new compounds include a ring system, which seems to be a pre-requisite for SDH inhibitors and bind to a hydrophobic portion of the active site. Additionally, hydroxyls, sulfonic or nitro functional groups interacted with the polar residues and the catalytic zinc atom. Vanillin azine and 3-hydroxy-2-napthoic(2-hydroxybenzylidene) hydrazide have comparable structures including hydroxyl groups and benzyl rings, while (+)-Amethopterin is an analogue of folic acid. The proposed interactions between the most active compound (flavin adenine dinucleotide disodium hydrate) and the active site residues of SDH are shown in Fig. 1.

Similar to SDI-158 [4], the potencies of the compounds *in vitro* are likely due to their interactions with the catalytic zinc. Additional interactions may include the stacking against the nicotinamide ring of NAD^+, the numerous van der Waals contacts and a small number of H-bonds between the compounds and the protein. The proposed models suggest that flavin adenine dinucleotide is coordinated to the zinc atom by oxygen and nitrogen atoms (1.8 Å and 1.9 Å, respectively) from the flavin ring which π-stacks against the nicotinamide ring of NAD^+ (Fig. 1). (+)-Amethopterin is H-bonded to His49 (3.0 Å) and Thr121 (2.9 Å). The zinc atom is likely coordinated by nitrogen atoms of the diamino-pteridin ring (3.2 Å and 3.9 Å). In case of the 3-hydroxy-2-napthoic(2-hydroxybenzylidene) hydrazide the zinc atom may be coordinated by a nitrogen atom from the 2-hydroxybenzylidene moiety (2.7 Å). Folic acid is H-bonded to Ser46 (3.7 Å), Thr121 (3.1 Å), Glu155 (2.8 Å) and Ser276 (2.3 Å), and may coordinate to the zinc atom through two nitrogens from its 4-pteridinol ring (3.2 Å and 3.8 Å). N-2,4-Dinitrophenyl-L-cysteic acid is likely coordinated through its sulfomethyl oxygen to the zinc atom (2.4 Å). Vanillin azine forms an H-bond with Thr121 (3.0 Å) and may coordinate to the zinc atom through an imine nitrogen (2.4 Å). In the case of 1H-indole-2,3-dione,5-bromo-6-nitro-1-(2,3,4-tri-O-acetyl-α-L-arabinopyranosyl)-(9Cl), the zinc atom is likely coordinated by an ester oxygen (2.3 Å).

This was the first study on the discovery of potential SDH inhibitors from virtual screening and resulted in a 33% success rate. From a total of 21 compounds tested 7 compounds were found to inhibit SDH with IC_{50} values in the micro molar range. Similar studies performed on the much more investigated aldose reductase, the first enzyme of the polyol pathway, have resulted in a similar success rate [17].

Table 1. **IC$_{50}$ Values, Molecular Formulae and Chemical Structures of SDI-158 and the Seven SDH Inhibitors Identified from the NCI Database**

Compound	Molecular Formula	IC$_{50}$ (µM)	Structure
SDI-158	C$_{11}$H$_{17}$N$_5$O$_3$	1	
Flavin adenine dinucleotide disodium hydrate	C$_{27}$H$_{33}$N$_9$O$_{15}$P$_2$	0.19	
(+)-Amethopterin	C$_{20}$H$_{22}$N$_8$O$_5$	1.1	
3-Hydroxy-2-napthoic(2-hydroxybenzylidene) hydrazide	C$_{18}$H$_{14}$N$_2$O$_3$	1.2	
Folic acid	C$_{19}$H$_{19}$N$_7$O$_6$	4.5	
N-2,4-Dinitrophenyl-L-cysteic acid	C$_9$H$_{10}$N$_3$NaO$_9$S	5.3	

(Table 1. Contd....)

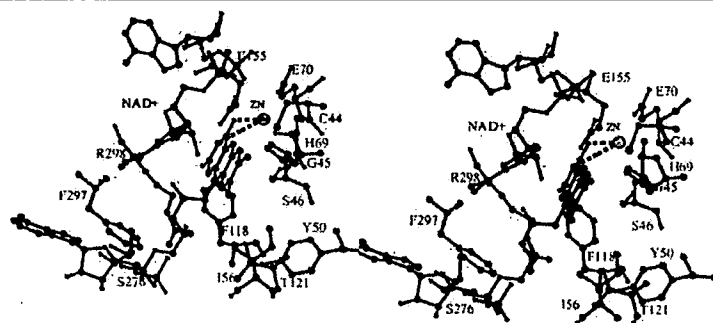| Compound	Molecular Formula	IC₅₀ (µM)	Structure
Vanillin azine	C₁₆H₁₆N₂O₄	7	
1H-Indole-2,3-dione,5-bromo-6-nitro-1-(2,3,4-tri-O-acetyl-α-L-arabinopyranosyl)-(9CI)	C₁₉H₁₇BrN₂O₁₁	28	

Fig. (1). Stereoview of the most active compound (flavin adenine dinucleotide disodium hydrate) identified from the NCI database and its proposed interactions with the SDH active site. Residues within 4 Å of the compound, H-bonds and the proposed coordination between the zinc atom and the compound (dashed lines) are shown.

REFERENCES

[1]   Jedziniak, J.A.; Chylack, L.T.; Cheng, H.-M.; Gillis, M.K.; Kalustian, A.A.; Tung, W.H. *Invest. Ophthalmol. Visual Sci.,* 1981, *20,* 314.
[2]   Ohkubo, Y.; Kishikawa, H.; Araki, E.; Miyata, T.; Isami, S.; Motoyoshi, S.; Kojima, Y.; Furuyoshi, N.; Shichiri, M. *Diabetes Res. Clin. Pract.,* 1995, *28,* 103.
[3]   Obrosova, I.G.; Fathallah, L.; Lang, H.J.; Greene, D.A. *Diabetologia,* 1999, *42,* 1187.
[4]   Pauly, T.; Ekstrom, J.; Beebe, D.; Chrunyk, B.; Cunningham, D.; Griffor, M.; Kamath, A.; Lee, E.; Madura, R.; Mcguire, D.; Subashi, T.; Wasilko, D.; Watts, P.; Mylari, B.; Oates, P.; Adams, P.; Rath, V. *Structure,* 2003, *11,* 1071.
[5]   Johansson, K.; El-Ahmad, M.; Kaiser, C.; Jörnvall, H.; Eklund, H.; Höög, J.; Ramaswamy, S. *Chemico-Biol. Interact.,* 2001, *130,* 351.
[6]   Banfield, M.; Salvucci, M.; Baker, E.; Smith, C. *J. Mol. Biol.,* 2001, *306,* 239.
[7]   Eklund, H.; Nordström, B.; Zeppezauer, E.; Söderlund, G.; Ohlsson, I.; Boiwe, T.; Söderberg, B.-O.; Brändén, C.; Åkeson, A. *J. Mol. Biol.,* 1976, *102,* 27.

[8]   Varlet, D.; Fourmaintraux, E.; Depreux, P.; Lesieur, D. *Heterocycles,* 2000, *53,* 797.
[9]   Chu-Moyer, M.; Ballinger, W.E.; Beebe, D.A.; Berger, R. ; Coutcher, J.B.; Day, W.W.; Li, J.; Mylari, B.L.; Oates, P.J.; Weekly, R.M. *J. Med. Chem.,* 2002, *45,* 511.
[10]   Mylari, B.L.; Oates, P.J.; Zembrowski, W.J.; Beebe, D.A.; Conn, E.L.; Coutcher, J.B.; Linhares, M.C.; Withbroe, G.J. *J. Med. Chem.,* 2002, *45,* 4398.
[11]   Schoichet, B; Bodian, D; Kuntz, I. *J. Comp. Chem.,* 1992, *13,* 380.
[12]   Meng, E.C.; Shoichet, B.K.; Kuntz, I.D. *J. Comput. Chem.,* 1992, *13,* 505.
[13]   Shoichet, B.K.; Kuntz, I.D. *J. Mol. Biol.,* 1991, *221,* 327.
[14]   Mine, G.W.A.; Nicklaus, M.C; Driscoll, J.S.; Wang, S.; Zaharatiz, D. *J. Chem. Inf. Comput. Sci.,* 1994, *34,* 1219.
[15]   Iwata, T.; Popescu, N.C.; Zimonjic, D.B.; Karlsson, C.; Höög, J.-O.; Vaca, G.; Rodriguez, I.R.; Carper, D. *Genomics,* 1995, *26,* 55.
[16]   Darmanin, C.; Iwata, T.; Carper, D.A.; Sparrow, L.G.; Chung, R.P.-T.; El-Kabbani, O. *Acta Cryst.,* 2002, *D58,* 1379.
[17]   Iwata, Y.; Arisawa, M.; Hamada, R.; Kita, Y.; Mizutani, M.Y.; Tomioka, N.; Itai, A.; Miyamoto, S. *J. Med. Chem.,* 2001, *44,* 1718.
[18]   Kraulis, P.J. *J. Appl. Cryst.,* 1991, *24,* 946.

Involvement of Insulin-like Growth Factor-I and Insulin-like Growth Factor Binding Protein-3 in Corneal Fibroblasts during Corneal Wound Healing

Kanako Izumi,[1,2] Daijiro Kurosaka,[1] Takeshi Iwata,[2] Yoshihisa Oguchi,[1] Yasuhiko Tanaka,[2] Yukihiko Mashima,[1] and Kazuo Tsubota[1]

PURPOSE. The involvement of downstream messengers of transforming growth factor (TGF)-β in the differentiation of corneal fibroblasts into myofibroblasts was investigated. The effects of insulin-like growth factor (IGF)-I and insulin-like growth factor binding protein (IGFBP)-3 upregulated by TGF-β were examined in human corneal fibroblasts, and the possible involvement of IGF axis components in corneal wound healing was assessed in a mouse model.

METHODS. Human corneal fibroblasts were incubated with TGF-β2 or IGF-I, to investigate IGF-I, IGF-II, IGFBP-3, type I collagen, and α-smooth muscle actin (α-SMA) mRNA, as well as IGFBP-3 protein expression, during myofibroblast differentiation. DNA synthesis was evaluated with a 5-bromo-2'-deoxyuridine (BrdU) incorporation assay. IGFBP-3 mRNA expression, protein expression, and immunolocalization were investigated in mouse corneas after photorefractive keratectomy (PRK).

RESULTS. TGF-β2 treatment induced expression of IGF-I and IGFBP-3 mRNA and of IGFBP-3 protein in human corneal fibroblasts. TGF-β2 and IGF-I both stimulated expression of type I collagen. TGF-β2 but not IGF-I potently stimulated α-SMA mRNA expression. IGF-I potently stimulated basal DNA synthesis, whereas IGFBP-3 inhibited it. IGF-I potently stimulated proliferation of TGF-β2-activated myofibroblasts without reversing the activated fibrogenic phenotype, whereas IGFBP-3 suppressed IGF-I-induced proliferation of corneal fibroblasts. IGFBP-3 mRNA and protein increased in mouse corneas soon after PRK, when in vivo immunostaining of the corneas showed expression of IGFBP-3 in the deep layer of the corneal stroma.

CONCLUSIONS. These results suggest that during corneal wound healing, TGF-β stimulates IGF axis components, whereas IGFBP-3 may modulate IGF-I-induced myofibroblast proliferation to suppress corneal mesenchymal overgrowth. (*Invest Ophthalmol Vis Sci.* 2006;47:591–598) DOI:10.1167/iovs.05-0097

During corneal wound healing leading to scar formation, keratocytes are activated, turn into fibroblasts, and eventually transformed to α-smooth muscle actin (α-SMA)-expressing myofibroblasts.[1-5] Myofibroblasts are central to wound healing, as they generate the contractile forces necessary for wound closure.[4,6,7] However, regulation of myofibroblast differentiation and proliferation is crucial, because an excessive number of myofibroblasts results in excessive scar formation.[8] Soluble mediators of wound repair, such as growth factors, are important in regulating myofibroblast differentiation and proliferation.

The differentiation of keratocyte into myofibroblasts has been shown to be induced by TGF-β.[3-5,9] TGF-β isoforms regulate multiple biological processes including cell proliferation, extracellular matrix synthesis, angiogenesis, immune response, apoptosis, and differentiation.[7,10-12] They have been implicated in the pathogenesis of fibrosis, autoimmune diseases, cancer, and other disorders.[7,10-12] TGF-β is a pluripotent cytokine capable of inhibiting or stimulating cell growth, depending on the nature of the target cell.[13] TGF-β is a potent inhibitor of growth in a variety of epithelial cell types, whereas in stromal cells it stimulates cell growth.[12,13]

Growth-promoting and metabolic regulatory activities of insulin-like growth factor (IGF)-I and -II are modulated by a family of six high-affinity insulin-like growth factor binding proteins (IGFBPs) and mediated by two IGF receptors (IGF-IR and -IIR), particularly IGF-IR.[14-16] Modulation of IGF actions by IGFBP may be positive or negative, depending on tissue type and physiologic or pathologic states.[15,17-20]

IGFBP-3 is one of the six IGFBPs that regulate binding of IGF-I with the cognate IGF-I receptor tyrosine kinase.[20-23] By modulating the binding of IGF-I to its receptor, an individual IGFBP can either inhibit or augment IGF-I-stimulated growth.[21,24-27] IGFBP-3 is a 40- to 45-kDa glycoprotein produced locally in many tissues, where it serves important paracrine and autocrine functions in modulating cellular growth and apoptosis.[22,23,28] IGFBP-3 activity at the cellular level is regulated, not only by its rate of synthesis, but also by post-translational modification and proteolysis.[29] Several IGFBP-3 proteases have been identified, including plasmin, matrix metalloproteases, kallikreins, prostate-specific antigen, and cathepsin D. This proteolysis results in IGFBP-3 fragments with a low affinity for IGFs.[30,31] IGFBP-3, like IGFBP-1 and IGFBP-5, is capable of regulating cell growth independent of its effects on IGF-I-stimulated growth.[32] For example, IGFBP-3 inhibits replication and promotes apoptosis in various cell lines in an IGF-independent manner.[32] Not only IGF-I but TGF-β1 and TGF-β2 enhance IGFBP-3 mRNA and protein expression in both epithelial and stromal cell types.[33-35] The IGF system plays an important role in wound healing,[14,15] and both IGF-I and IGFBP-3 are present in wound fluid in significant concentrations.[14,15,19]

To our knowledge, the IGFBP-3 system has not been investigated in corneal wound healing. To test our hypothesis that IGF axis components regulate corneal scar formation, we investigated whether TGF-β2 induces IGF-I and IGFBP-3 expression and whether IGFBP-3 modulates IGF-I-induced myofibroblast proliferation in cultured corneal fibroblasts. We then evaluated expression and localization of IGFBP-3 in mouse cornea after photorefractive keratectomy (PRK).

MATERIALS AND METHODS

Cell Culture

Human corneal fibroblasts were isolated from corneal limbal rims donated by the Northwest Lions Eye Bank (Seattle, WA). Procedures used in this human-cell in vitro research conformed to the tenets of the Declaration of Helsinki. Corneal tissue was cut into pieces and incubated in a humidified atmosphere of 5% CO_2 and 95% air at 37°C in Dulbecco's modified Eagle's medium (DMEM; Invitrogen-Gibco, Grand Island, NY) containing 10% fetal bovine serum (FBS; Invitrogen-Gibco). Cells in the third passage were used for experiments. The purity of cell cultures was assessed by determining the reactivity with antibodies to vimentin by immunofluorescence analysis. All fibroblasts were immunoreactive for vimentin but not for cytokeratin, suggesting the absence of contamination by epithelial cells.

For reverse-transcription polymerase chain reaction (RT-PCR) experiments, human corneal fibroblasts were cultured at a density of 6.0×10^4/mL in serum-free medium. After 24 hours, this medium was replaced with serum-free medium containing TGF-β2 (0.01–100 ng/mL; R&D Systems, Minneapolis, MN), IGF-I (50 ng/mL; R&D Systems), and anti-IGF-I neutralizing antibody (20 μg/mL; R&D Systems). Incubation was continued for 12, 24, 48, or 72 hours before RNA was extracted for analysis.

For Western blot analysis, human corneal fibroblasts were cultured at a density of 6.0×10^5/mL in serum-free medium. After 24 hours, this medium was replaced with serum-free medium containing 1 ng/mL TGF-β2 for incubations continuing a further 12, 24, 48, or 72 hours before collection of medium for analysis. The conditioned medium was collected, centrifuged to remove cell debris, and stored at −80°C until use.

Photorefractive Keratectomy

Animal procedures were performed in accordance with the ARVO Statement for the Use of Animals in Ophthalmic and Vision Research. Six- to 8-week-old mice (C57BL/6) were used. To induce corneal wounds, first we anesthetized mice by an intraperitoneal injection of 10% pentobarbital (0.15 mg/10 g body weight). A drop of proparacaine HCl (0.05%) was applied to the eye, and the cornea was centered under the laser microscope. Two-millimeter corneal wounds were produced in the right eye of each animal by transepithelial excimer laser abrasion (2-mm optical zone; 42- to 44-μm ablation depth; PTK mode; model EC5000; Nidek, Yokohama, Japan). After excimer laser treatment, tobramycin ointment (0.3%) was applied to the corneal surface to prevent infection. No postoperative topical steroid was administered. At 12 hours and 1, 3, 7, and 14 days after excimer laser ablation, mice were euthanatized for excision of corneas under an operating microscope, these were stored at −80°C until analysis. Thirteen mice were euthanatized at each time point. Five mice at each time point were used for RNA analysis, five for Western blot analysis, and three for immunohistochemistry. Eight corneas from four mice that did not undergo excimer ablation were used as the normal control (day 0).

RNA Extraction

Total RNA was extracted from pooled corneas or cultured fibroblasts after various experimental manipulations. Homogenization was performed in extraction reagent (TRIzol; Invitrogen). Total RNA was extracted from each sample by chloroform, precipitated with isopropanol, and washed with ethanol. RNA pellets were dissolved in diethylpyrocarbonate (DEPC)-treated water and stored at −80°C. The total RNA concentration was measured spectrophotometrically at 260 nm.

PCR Procedure

First-strand cDNA was synthesized with reverse transcriptase (Super-Script II; Invitrogen) and random primer, together with 1 μg of total RNA from the sample. For RT-PCR, gene-specific primers were de-

signed by computer (Primer Express software; Applied Biosystems, Inc., [ABI] Foster City, CA) on the basis of full-length cDNA sequence data (provided by Celela Discovery Systems; ABI). These were as follows: for human IGFBP-3, 5′-CCCAACTGTGACAAGAAGGGATT-3′ (forward primer) and 5′-CAGGCGTCTACTTGCTCTGCAT-3′ (reverse primer); for mouse IGFBP-3, 5′-CCATCCACTCCAT GCCAAGA-3′ (forward primer) and 5′-GGGACTCAGCACATTGAGGAA-3′ (reverse primer); for human IGF-I, 5′-CACCATGTCCTCCTCGCATCT-3′ (forward primer) and 5′-ATCCACGATGCTGTCTGAGG-3′ (reverse primer); for human IGF-II, 5′-CCTGGAGACGTACTGTGCTACC-3′ (forward primer) and 5′-GCTCACTTCCGATTGCTGG-3′ (reverse primer); for human procollagen-α1(I), 5′-AGTCACCCACCGACCAAGAAA-3′ (forward primer) and 5′-CATAAGACAGCTGGGGAGCAAA-3′ (reverse primer); for human α-SMA, 5′-CCAACTGGGACGACATGGAAA-3′ (forward primer) and 5′-GCGTCCAGAGGCATAGAGAGACA-3′ (reverse primer); for human GAPDH, 5′-CAGCCTCAAG ATCATCAGCAAT-3′ (forward primer) and 5′-GGTCATGAGTCCTTCCACGATAC-3′(reverse primer); and for mouse 18S 5′-GATCGAAGACGATCAGATACC-3′ (forward primer) and 5′-CCAGA CAAATCACTCCACC-3′ (reverse primer). The last two of these were used as the endogenous control. Real-time quantitative PCR was performed with a commercial system (model 5000; ABI). Volumes of 50 μL were used for reactions in 96-well plates. The amplification protocol specified incubation at 50°C for 2 minutes and at 95°C for 10 minutes, followed by 40 cycles at 95°C for 15 seconds and 60°C for 1 minute. The PCR cycle number (C_T) at which fluorescence emission reached a threshold value above baseline emission was used to quantitate the original amount of each mRNA, which was normalized to the amount of human GAPDH or mouse 18S.

IGFBP-3 Immunohistochemistry in Mouse Corneal Sections

Eyes harvested at each time point were incubated in 4% paraformaldehyde and phosphate-buffered saline (PBS) overnight at 4°C. Paraffin-embedded sections were cut at a 4-μm thickness and affixed to glass slides (Superfrost; Matsunami, Osaka, Japan). Formalin-fixed paraffin-embedded sections of tissue were heated, dewaxed, and rehydrated before blocking of endogenous peroxidase (0.1%, vol/vol hydrogen peroxide). Sections were incubated with polyclonal rabbit antibody against mouse IGFBP-3 (GroPep, Adelaide, Australia). Specific binding was detected by an Alexa 488-conjugated anti-rabbit secondary antibody (Molecular Probes, Eugene, OR). The sections were counterstained with propidium iodine, and mounted in anti-fading solution (Vector Laboratories, Burlingame, CA). In addition to the fluorescent conjugate, primary antibody was detected with an immunoperoxidase protocol (Envision kit; Dako, Ely, UK). Fluorescent images were photographed with a laser scanning confocal microscope (LSM510; Carl Zeiss Meditec, Jena, Germany).

Western Blot Analysis

For Western blot analysis, 10 mL serum-free conditioned medium collected from each flask was concentrated by centrifugation in a spin column (Centricon 50; Millipore, Bedford, MA) to achieve a 200-fold concentration. Protein from the concentrated conditioned medium of corneal fibroblasts or protein extracted from mouse cornea after PRK was analyzed for IGFBP-3 on 15% SDS-polyacrylamide gels and then electrophoretically transferred to polyvinylidene difluoride (PVDF) membrane. Overall protein concentrations were determined by the Lowry assay. Transfer was performed at a constant voltage of 60 V for 1 hour. After transfer, the membrane was incubated in Tris-buffered saline (TBS) containing 5% skim milk for 1 hour at room temperature. The membrane was rinsed three times with TBS-0.1% Tween, and then incubated with an anti-human IGFBP-3 monoclonal antibody (R&D Systems) or a polyclonal rabbit antibody against mouse IGFBP-3 (GroPep) for 2 hours at room temperature. The membrane was rinsed with TBS-0.1% Tween and then incubated with horseradish peroxidase-labeled goat anti-rabbit IgG (Jackson ImmunoResearch Laborato-